Estimating global surface ammonia concentrations inferred from satellite retrievals

Lei Liu [a, b, c, *], Xiuying Zhang [b, *], Anthony Y.H. Wong [c], Wen Xu [d], Xuejun Liu [d], Yi Li [e], Huan Mi [c, f], Xuehe Lu [b], Limin Zhao [b], Zhen Wang [b], Xiaodi Wu [b, g], Jing Wei [h]

[a] College of Earth and Environmental Sciences, Lanzhou University, Lanzhou 730000, China

[b] International Institute for Earth System Science, Nanjing University, Nanjing, 210023, China

[c] Department of Earth and Environment, Boston University, Boston, Massachusetts, USA

[d] College of Resources and Environmental Sciences, Centre for Resources, Environment and Food Security, Key Lab of Plant-Soil Interactions of MOE, China Agricultural University, Beijing, 100193, China

[e] Sunset CES Inc., Beaverton, OR, 97008, USA

[f] College of Surveying and Geo-Informatics, Tongji University, 1239 Siping Road, Shanghai, China

[g] Jiangsu Center for Collaborative Innovation in Geographical Information Resource Development and Application, Nanjing, 210023, China

[h] State Key Laboratory of Remote Sensing Science, College of Global Change and Earth SystemScience, Beijing Normal University, Beijing, China,

* Correspondence to Lei Liu (liuleigeo@lzu.edu.cn) and Xiuying Zhang (zhangxy@nju.edu.cn).

Abstract

Ammonia (NH_3), as an alkaline gas in the atmosphere, can cause direct or indirect effects on the air quality, soil acidification, climate change as well as human health. Estimating surface NH_3 concentrations is critically important for modelling the dry deposition of NH_3 and for modelling the formation of ammonium nitrate, which have

important impacts on the natural environment. However, sparse monitoring sites make it challenging and difficult to understand the global distribution of surface NH_3 concentrations both in time and space. We estimated the global surface NH_3 concentrations for the years of 2008-2016 using the satellite NH_3 retrievals combining its vertical profiles from the GEOS-Chem. The accuracy assessment indicates that the satellite-based approach has achieved a high predictive power for annual surface NH_3 concentrations compared with the measurements of all sites in China, US and Europe (R^2=0.76 and RMSE=1.50 μg N m^{-3}). The satellite-derived surface NH_3 concentrations had higher consistency with the ground-based measurements in China (R^2=0.71 and RMSE=2.6 μg N m^{-3}) than the US (R^2=0.45 and RMSE=0.76 μg N m^{-3}) and Europe (R^2=0.45 and RMSE=0.86 μg N m^{-3}) at a yearly scale. Annual surface NH_3 concentrations higher than 6 μg N m^{-3} are mainly concentrated in the North China Plain of China and Northern India, followed by 2-6 μg N m^{-3} mainly in southern and northeastern China, India, western Europe and eastern United States (US). High surface NH_3 concentrations were found in the croplands in China, US and Europe, and surface NH_3 concentrations in the croplands in China were approximately double than those in the croplands in the US and Europe. The linear trend analysis shows that an increase rate of surface NH_3 concentrations (>0.2 μg N m^{-3} y^{-1}) appeared in the eastern China during 2008-2016, and a middle increase rate (0.1-0.2 μg N m^{-3} y^{-1}) occurred in northern Xinjiang over China. NH_3 increase was also found in agricultural regions in middle and eastern US with an annual increase rate of lower than 0.10 μg N m^{-3} y^{-1}. The satellite-derived surface NH_3 concentrations help us to determine the NH_3 pollution status in the areas without monitoring sites and to estimate the dry deposition of NH_3 in the future.

Introduction

Ammonia (NH_3), emitted primarily by agricultural activities and biomass burning, is an important alkaline gas in the atmosphere (Van Damme et al., 2018;Warner et al., 2017). Excessive surface NH_3 concentrations can cause chronic or acute damage to the plant (such as reduced growth and bleached gray foliage) when its capacity of

57 detoxification is exceeded (Eerden, 1982;Sheppard et al., 2008). Estimation of surface
58 NH_3 concentrations is critically important in modelling the dry deposition of NH_3,
59 which may comprise a large part of atmospheric nitrogen (N) deposition, and could
60 cause acidification in the soil, eutrophication in the aquatic ecosystems, and
61 contamination in drinking water (Basto et al., 2015;Kim et al., 2014;Lamarque et al.,
62 2005;Larssen et al., 2011;Reay et al., 2008). In addition, NH_3 can also react with
63 nitric acid and sulfuric acid to form ammonium salts (Li et al., 2014;Li et al., 2017b),
64 which are important components of particulate matters (PM), and have negative
65 impacts on air quality and human health (Xu et al., 2017;Schaap et al., 2004;Wei et al.,
66 2019).
67 Several national monitoring programs can measure surface NH_3 concentrations,
68 including the Chinese Nationwide Nitrogen Deposition Monitoring Network
69 (NNDMN) established in 2004, the Ammonia Monitoring Network in China
70 (AMoN-China) established in 2015 in China, the Ammonia Monitoring Network in
71 the US (AMoN-US) as well as the European Monitoring and Evaluation Programme
72 (EMEP). However, there are still relatively large uncertainties of estimating global
73 surface NH_3 concentrations, resulting from the sparse monitoring sites as well as the
74 limited spatial representativeness (Liu et al., 2017b;Liu et al., 2017a). Satellite NH_3
75 retrievals are an important complement to gain the global distribution of NH_3
76 concentrations with a high spatial resolution (Van Damme et al., 2014c). NH_3 can be
77 measured by several satellite instruments including the Infrared Atmospheric
78 Sounding Interferometer (IASI), Atmospheric Infrared Sounder (AIRS), Cross-track
79 Infrared Sounder (CrIS) and Tropospheric Emission Spectrometer (TES). TES using
80 the thermal infrared spectral range has sparser spatial coverage compared to IASI,
81 CrIS and AIRS (Shephard et al., 2011;Zhang et al., 2017a). A recent study (Kharol et
82 al., 2018) reported the dry NH_3 depositions in North America, and found -15%
83 underestimation in CrIS surface NH_3 concentrations (using three fixed NH_3 profiles
84 considering unpolluted, moderate and polluted conditions) compared with the
85 measurements from the AMoN-US during the warm months (from April to
86 September). Warner et al. reported the global AIRS NH_3 concentrations at 918hPa

(approximately 700-800 m) at 1° latitude × 1° longitude grids, and found NH_3 concentrations increased in the major agricultural regions during 2003-2015 (Warner et al., 2017). The IASI NH_3 measurements have been validated with NH_3 columns measured by the Fourier transform infrared spectroscopy (FTIR), ground-based NH_3 measurements, NH_3 emissions and atmospheric chemistry transport models (CTMs) (Dammers et al., 2016;Van Damme et al., 2014c;Van Damme et al., 2014a;Whitburn et al., 2016).

Apart from satellite retrievals, CTMs are also powerful tools to investigate spatiotemporal variability of surface NH_3 concentrations in the atmosphere. Schiferl et al. evaluated the modelled NH_3 concentrations during 2008-2012 from GEOS-Chem, and found an approximately 26% underestimation compared with the ground-based measurements, which can be related to the relatively large uncertainties in NH_3 emissions used for driving GEOS-Chem (Schiferl et al., 2015). Zhu et al. used the GEOS-Chem constrained by TES measurements to estimate surface NH_3 concentration during 2006-2009, and found an improvement in comparison with the ground-based measurements in the United States (Zhu et al., 2013). Schiferl et al. used the airborne observations to validate the simulated NH_3 concentrations in 2010 from GEOS-Chem, and revealed reasonably simulated NH_3 vertical profiles compared with the aircraft measurements but with an underestimation in surface NH_3 concentrations in California (Schiferl et al., 2014). A number of previous studies have used satellite NO_2 columns to estimate the surface NO_2 concentrations combining NO_2 vertical profiles from CTMs (Geddes et al., 2016;Lamsal et al., 2013;Nowlan et al., 2014;Liu et al., 2017c). The methods of using the vertical profiles to convert satellite-retrieved columns to surface concentrations have been proven successful for SO_2 and NO_2 (Geddes et al., 2016;Geng et al., 2015;Lamsal et al., 2008;Nowlan et al., 2014). CTMs can provide valuable information of NH_3 vertical profiles (Whitburn et al., 2016;Liu et al., 2017b), and IASI-derived surface NH_3 concentrations combining NH_3 vertical profiles from CTMs in China and Europe were evaluated previously (Liu et al., 2017b;Graaf et al., 2018). This study followed these studies to estimate the satellite-derived global surface NH_3 concentrations using IASI NH_3 retrievals and the

vertical profiles from GEOS-Chem, and the present study aims to estimate the global surface NH_3 concentration from a satellite perspective.

Data and Methods

IASI NH_3 measurements

The Infrared Atmospheric Sounding Interferometer (IASI) is a passive instrument measuring infrared radiation within the spectral range of 645-2769 cm^{-1}. The IASI-A instrument is on board of the MetOp-A satellite launched in 2006 covering the globe twice a day with an elliptical spatial resolution of approximately 12 by 12 kilometers, and cross the equator at 09:30 and 21:30 local times (Van Damme et al., 2014b). We used the daytime IASI NH_3 measurements due to the larger positive thermal contrast detected by satellite instruments leading to smaller errors compared to the nighttime data (Van Damme et al., 2014b). In this work, we used the IASI NH_3 columns products (ANNI-NH3-v2.2R-I) during 2008-2016 (Van Damme et al., 2017) to estimate the global surface NH_3 concentrations. The ANNI-NH3-v2.2R-I datasets were developed by converting spectral HRI (hyperspectral range index) to NH_3 columns through an Artificial Neural Network for IASI (ANNI) algorithm (Whitburn et al., 2016). This algorithm considered the influence of the NH_3 vertical profiles, pressure, humidity and temperature profiles. The NH_3 vertical profile information used to generate the ANNI NH_3 columns were retrieved from GEOS-Chem, which integrates H_2SO_4-HNO_3-NH_3 aerosol thermodynamics mechanism (Whitburn et al., 2016;Van Damme et al., 2017). The ANNI-NH3-v2.2R-I datasets used the ANNI algorithm and took account of the influence of NH_3 vertical profiles, pressure, humidity and temperature profiles, which was to make the columns accurate. There is no information on NH_3 vertical profiles in the ANNI-NH3-v2.2R-I datasets. The NH_3 vertical profiles used in this paper was to convert the columns to surface concentrations and to make the surface NH_3 estimates accurate. The IASI NH_3 columns used in this study were processed into the monthly data at 0.25 ° latitude × 0.25 ° longitude grids by the arithmetic averaging method (Van Damme et al.,

2017;Whitburn et al., 2016;Liu et al., 2017a).

Surface NH_3 measurements

To evaluate our satellite-derived global surface NH_3 concentrations, we collected available surface NH_3 measurements on a regional scale in 2014. In China, we used the national measurements from the Chinese Nationwide Nitrogen Deposition Monitoring Network (NNDMN) including 10 urban sites, 22 rural sites, and 11 background sites. Surface NH_3 concentrations in the NNDMN were measured by both ALPHA (Adapted Low-cost, Passive High Absorption) and DELTA (Denuder for Long-Term Atmospheric sampling) systems. The bias for monthly measurements at a site using DELTA systems is as below approximately 10% (Sutton et al., 2001), and the correlation between the ALPHA and DELTA measurements was highly significant (R^2=0.919, p<0.001) (Xu et al., 2015). The detailed descriptions on the NNDMN have been described in a previous study (Xu et al., 2015). In the US, we used the measurements of 67 sites from the AMoN-US, downloaded from the website: http://nadp.sws.uiuc.edu/AMoN/. Surface NH_3 concentrations in the AMoN-US were measured by the radiello diffusive sampler (http://www.radiello.com) as a simple diffusion-type sampler collected every 2 weeks, and these sites were generally distributed at rural sites (Li et al., 2016). We calculated annual surface NH_3 concentrations by averaging all the measurements since we compared the measured surface NH_3 concentrations with satellite-derived surface NH_3 concentrations at a yearly scale. In Europe, we used the measurements of 43 sites from the EMEP network (https://www.nilu.no/projects/ccc/emepdata.html). The EMEP is composed of multiple national networks in Europe, thus the measurement systems differs among different national networks. The overall bias of the different instruments in EMEP varied from -30 to 10% for all sites (Bobrutzki et al., 2010). Most sites in China, US and Europe were set a height of 1-50 m above the ground (Xu et al., 2015;Li et al., 2016;Puchalski et al., 2011).

GEOS-Chem model

We used GEOS-Chem version 11-01 as the chemical transport model to calculate global NH_3 vertical profiles (using the year of 2014 as a case study in the results and discussion). We did the spin up for 5 months, which well exceed the typical lifetime of atmospheric NH_3 (typically within 24 hours) and aerosol ammonium ions (typically within a week) (Pye et al., 2009). It has a spatial resolution of 2° latitude $\times$ 2.5° longitude $\times$ 47 vertical layers spanning over Earth's surface and about 80 km above it. It is driven by the meteorological field data of the GEOS-FP (forward-processing) products, which were produced by NASA GMAO (Global Modelling and Assimilation Office) (https://gmao.gsfc.nasa.gov/). Here we modelled the NH_3 vertical profiles using GEOS-Chem, and used the monthly averages for analysis. The global NH_3 emissions in GEOS-Chem are based on the EDGAR (Emissions Database for Global Atmospheric Research) v4.2 (http://edgar.jrc.ec.europa.eu/overview.php?v=42), while the regional emissions are replaced with MIX inventory for East Asia (Li et al., 2017a) (http://www.meicmodel.org/dataset-mix.html), EMEP inventory for Europe (http://www.emep.int/), NEI (National Emissions Inventory, 2011) for the US (https://www.epa.gov/air-emissions-inventories) and CAC (Criteria Air Contaminant) inventory for Canada (https://www.canada.ca/en/services/environment/pollution-waste-management/national-pollutant-release-inventory.html). The main difference between the regional inventories and EDGAR is that seasonality of emissions is included in regional inventories. The seasonality of regional emissions inventories is embedded as integral part of the inventory except EMEP (Janssens-Maenhout et al., 2015;Crippa et al., 2018;Lenhart and Friedrich, 1995). The biomass burning emissions are from Global Fire Emissions Database (GFED4) including agricultural fires, wildfire and pre-scribed burning (Giglio et al., 2013). The GEOS-Chem simulates a comprehensive atmospheric NO_x-O_3-VOC-aerosol system (Mao et al., 2013). The thermodynamic equilibrium of NH_3-H_2SO_4-HNO_3 system is simulated by the

ISORROPIA II model (Fountoukis and Nenes, 2007;Pye et al., 2009). The modelling of wet deposition is described by a previous study (Liu et al., 2001) with updates from the studies (Amos et al., 2012;Wang et al., 2011). Dry deposition of particles follows the size-segregated treatment (Zhang et al., 2001) and gaseous dry deposition follows the framework (Wesely, 1989) with updates from a previous study (Wang et al., 1998). We archive the output daily averages of NH_3 concentrations as well as the averages between 9 and 10 am, which corresponds to the local crossing time of IASI (9:30 am). The local time is the time in a particular region or area expressed with reference to the meridian passing through it. The relationship between NH_3 concentration at 9-10 am and the daily averages derived from the GEOS-Chem was used to convert the satellite observed NH_3 column to daily averages (Nowlan et al., 2014).

Estimation of surface NH_3 concentrations

We estimated global surface NH_3 concentrations using the IASI NH_3 columns as well as the GEOS-Chem. We took into account the advantages of IASI NH_3 columns with high spatial resolutions and the GEOS-Chem with vertical profiles. The IASI NH_3 data we gained are column data, and there is no information on the vertical information. To convert the columns to surface concentrations, we used the widely used modelled vertical profiles from GEOS-Chem. The GEOS-Chem outputs include 47 layers, which are not continuous in the vertical direction. To gain the continuous vertical NH_3 profile, we used the Gaussian function to fit the 47 layers' NH_3 concentrations. The main advantage to simulate the vertical profiles is that the NH_3 concentration at any height indicated by satellite can be obtained. On the other hand, the simulated profile function has a general rule, which can convert the columns indicated by satellite to surface concentration simply and quickly for many years. The height of each grid box used here was calculated at the middle height of each layer rather than the top height of each layer. A three-parameter Gaussian function was used to fit NH_3 vertical profiles at each grid box from the GEOS-Chem in the previous studies (Whitburn et al., 2016;Liu et al., 2017b) :

$$\rho = \rho_{max} e^{-(\frac{Z-Z_0}{\sigma})^2} \quad (1)$$

where ρ is NH_3 concentrations at the layer height Z; ρ_{max} is the maximum NH_3 concentrations at the height z_0; σ is an indicator for the spread or thickness of the NH_3 concentrations.

This study expanded the equation (1) to fit NH_3 vertical profiles at each grid box by the following equation (Liu et al., 2017b):

$$\rho = \sum_{i=1}^{n} \rho_{max,i} e^{-(\frac{Z-Z_{0,i}}{\sigma_i})^2} \quad (2)$$

where n ranges from 1 to 6. If n equals 1, the equation (2) is the same as the equation (1); if n is greater than 1, the equation (2) is the multiple three-parameters Gaussian items. We determined the value of n that can simulate the NH_3 vertical profiles with best performance at each grid box using the determining coefficients of R-Square (R^2). Once the NH_3 vertical profiles were determined at each grid box, we can extrapolate NH_3 concentrations at any height from the GEOS-Chem ($G_{GEOS-Chem}$).

We then aggregated the IASI NH_3 columns Ω_{IASI} (0.25 ° latitude × 0.25 ° longitude) to the GEOS-Chem grid size $\overline{\Omega_{IASI}}$ (2 ° latitude × 2.5 ° longitude) by the averaging method. We have the following equation (Lamsal et al., 2008):

$$\overline{G_{IASI_{9-10}}} = \frac{G_{GEOS-Chem}}{\Omega_{GEOS-Chem}} \times \overline{\Omega_{IASI_{9-10}}} \quad (3)$$

where $\overline{G_{IASI_{9-10}}}$ is the satellite-derived surface NH_3 concentrations at a GEOS-Chem grid size at 9-10am; $\frac{G_{GEOS-Chem}}{\Omega_{GEOS-Chem}}$ is the ratio of surface NH_3 concentrations to NH_3 columns calculated from GEOS-Chem; $\overline{\Omega_{IASI_{9-10}}}$ is the average IASI NH_3 columns at a GEOS-Chem grid at 9-10am.

We found a high correlation (R=0.96 and p=0.000) between the surface NH_3 concentrations and NH_3 columns based on the GEOS-Chem outputs (**Fig. S1**). Then we used the satellite-derived scaling factor to downscale the satellite-derived surface NH_3 concentrations at a GEOS-Chem grid by using the following ratio:

$$R_{IASI} = \frac{\Omega_{IASI}}{\overline{\Omega_{IASI}}} \quad (4)$$

$$G_{IASI_{9-10}} = \overline{G_{IASI_{9-10}}} \times R_{IASI} \quad (5)$$

where R_{IASI} is the scaling factor. $G_{IASI_{9-10}}$ is the satellite-derived surface NH_3 concentrations at a satellite IASI grid size (0.25 °latitude ×0.25 °longitude) at 9-10am. To convert the instantaneous satellite-derived surface NH_3 concentrations G_{IASI} to daily average surface NH_3 concentrations, we followed the methods (Nowlan et al., 2014):

$$G_{IASI}{}^{*}=\frac{G_{GEOS-Chem}^{1-24}}{G_{GEOS-Chem}^{9-10}} \times G_{IASI_{9-10}} \quad (6)$$

where $G_{IASI}{}^{*}$ is the daily average surface NH_3 concentrations, and $\frac{G_{GEOS-Chem}^{1-24}}{G_{GEOS-Chem}^{9-10}}$ is the ratio of the GEOS-Chem surface NH_3 concentrations at the daily average to the average of 9-10 am.

Results and Discussion

NH_3 vertical profiles from GEOS-Chem

NH_3 emitted from the surface can be transported horizontally or vertically, and its concentrations may show a certain gradient in the vertical and horizontal directions (Preston et al., 1997;Rozanov et al., 2005). There are generally two types of shapes of NH_3 vertical profiles (**Fig. S2**) from aircraft measurements (Li et al., 2017b;Tevlin et al., 2017) and CTMs (Whitburn et al., 2016;Liu et al., 2017b). One is representative for the vertical profile with maximum NH_3 concentrations at a certain height (z_0>0) and the other is representative for the vertical profile with maximum NH_3 concentrations near the earth surface (z_0=0). In this study, the vertical profiles of NH_3 were fitted based on the 47 layers' outputs by GEOS-Chem in 2014 at a monthly scale. **Fig. S3** shows the spatial distribution of NH_3 concentrations in the first and fifth layers simulated by GEOS-Chem in January 2014. NH_3 concentrations in the fifth layer are significantly lower than those in the first layer, suggesting that NH_3 concentrations decrease with increasing layers (or altitude), especially in NH_3 hotspot regions (such as eastern China, India, western Europe and eastern US). The average difference of NH_3 concentrations between the first and fifth layers on the land is 0.34 μg N m^{-3}. The average NH_3 concentrations in the first and fifth layers in eastern China,

India, western Europe and eastern US were 2.76, 7.28, 0.55 and 0.31 μg N m^{-3}, respectively.

To more vividly depict the vertical profiles of NH_3, we show NH_3 vertical concentrations with cross-section drawn at 37°N in January, 2014 (**Fig. S4**). High NH_3 concentrations are mainly concentrated in the 1-10 layers, and show a significant decrease trend with the increasing altitude, which is consistent with the aircraft measurements (Preston et al., 1997;Lin et al., 2014;Levine et al., 1980;Shephard and Cady-Pereira, 2015;Li et al., 2017b;Tevlin et al., 2017). NH_3 vertical profiles were fitted by Gaussian function (2-6 terms) based on the 47 layers' NH_3 concentrations from the GEOS-Chem, and the fitting accuracy was determined by R^2. We found that the NH_3 vertical profiles on the land between 60 °N and 55 °S can be well modelled using Gaussian function (R^2 higher than 0.90) (**Fig. 1**). Previous studies also found high accuracy using the Gaussian function to simulate the NH_3 vertical profiles in China and globally (Whitburn et al., 2016;Liu et al., 2017b).

Validation of satellite-derived surface NH_3 concentrations

NH_3 vertical profiles were used to convert IASI NH_3 columns to surface NH_3 concentrations. **Fig. 2** shows the IASI-derived global surface NH_3 concentrations on the land at 0.25 ° latitude × 0.25 ° longitude grids in 2014. IASI-derived surface NH_3 concentrations capture the general spatial pattern of surface NH_3 concentrations fairly well in 2014 in regions with relatively intensive monitoring sites (R^2=0.76 and RMSE=1.50 μg N m^{-3} in **Fig. 2 and Fig. 3**). Overall, 72.85% of observations (including China, the US and Europe) were within a factor of two of the satellite-derived surface NH_3 concentrations. In China, there is approximately 71.43% and 77.27% of observations were within a factor of two of the satellite-derived surface NH_3 concentrations in urban and rural land uses, respectively. There is no big difference in the accuracy of satellite-derived surface NH_3 concentrations between urban and rural land uses. In the US, the monitoring sites were generally distributed at rural sites (http://www.radiello.com) (Li et al., 2016), and, in Europe, there is no information to indicate the land use of each site (https://projects.nilu.no//ccc/)

(Tørseth et al., 2012a). The overall mean of satellite-derived surface NH_3 concentrations in 2014 at the measured sites was 2.52 μg N m^{-3} and was close to the average of measured surface NH_3 concentrations (2.51 μg N m^{-3}) in 2014. IASI-derived surface NH_3 concentrations gained higher consistency with the ground-based measurements in China (R^2=0.71 and RMSE=2.6 μg N m^{-3} for 43 sites) than the US (R^2=0.45 and RMSE=0.76 μg N m^{-3} for 67 sites) and Europe (R^2=0.45 and RMSE=0.86 μg N m^{-3} for 43 sites) at a yearly scale. This might be due to the fact that for high concentrations in a region (associated with high thermal contrast) can be more reliably detected by IASI (Van Damme et al., 2014a). The accuracy of IASI-retrieved surface NH_3 concentrations in different regions is highly linked with the thermal contrast (TC) and atmosphere NH_3 abundance (Whitburn et al., 2016). The lowest uncertainties occur when high columns and high TC coincide. In case either of them decreases, the uncertainty will gradually increase. In case both the TC and column are low, all sensitivity to NH_3 is lost. When high TC and high NH_3 columns (high HRI) occurs, the major contribution to the uncertainty results from the thickness of the NH_3 layer, the surface temperature as well as the temperature profile (Whitburn et al., 2016). The simulation of NH_3 mixing from GEOS-Chem may also have different accuracy in different regions, and thus can cause uncertainty to the different accuracy of IASI-retrieved surface NH_3 concentrations in different regions. Notably, we compared the surface NH_3 concentrations at the monitoring stations with the grid values of satellite-derived estimates directly. This point-to-grid verification strategy may cause uncertainty since the monitoring site location may not be representative of a given grid cell for an average retrieved value. The satellite-derived NH_3 has a detection limit of 0.0025 μg N m^{-3} (2.5 ppb) (Graaf et al., 2018;Van Damme et al., 2014a). Similarly, we also compared the surface NH_3 concentrations (at the first layer) simulated by GEOS-Chem with the monitoring results (R^2=0.54 and RMSE=2.14 μg N m^{-3} in **Fig. 3**). In general, IASI-derived surface NH_3 concentrations had better consistency with the ground-based measurements than those from GEOS-Chem over China, the US and Europe. The relatively low accuracy from GEOS-Chem was likely due to the coarse model resolutions as well as the poor

spatiotemporal representations of NH_3 emissions, as suggested by a previous study (Zhang et al., 2018).

A known limitation of IASI NH_3 retrievals is lack of the vertical profile information. A previous study (Van Damme et al., 2014a) used fixed profiles on the land to convert the IASI NH_3 columns to surface NH_3 concentrations. Using the fixed profiles can cause large uncertainties for estimating surface NH_3 concentrations. In this work, we utilized the advantages of CTMs and considered the spatial variability of the vertical profiles, and proves that IASI NH_3 columns are powerful to predict the surface NH_3 concentrations combining the vertical profiles simulated by Gaussian function.

Through the Gaussian simulation of NH_3 vertical profiles, we are able to evaluate the sensitive regions of surface NH_3 concentrations with respect to different heights. **Fig. S5** shows the spatial distribution of the difference of NH_3 concentrations between 40m and 60m (about the middle height of the first layer in GEOS-Chem). In general, in strong NH_3 emission regions, there is a relatively large difference in surface NH_3 concentrations such as, for instance, in eastern China and northwestern India (can be up to 3 μg N m^{-3}); subsequently, a middle difference (2-3 μg N m^{-3}) occurs in eastern and middle China, northern India and northern Italy. Except above mentioned regions, the difference of NH_3 concentrations between 40m and 60m is generally lower 0.5 μg N m^{-3}.

Spatial distributions of satellite-derived surface NH_3 concentrations

Fig. 4 shows the spatial distributions of surface NH_3 concentrations in China, US and Europe in 2014. The overall mean surface NH_3 concentrations over China were 2.38 μg N m^{-3}, with the range of 0.22-13.11 μg N m^{-3}. We found large areas in eastern China (109-122^{o} E, 28-41^{o} N), Sichuan Basin, Hubei (including Wuhan, Xiangyang and Yichang), Shaanxi (including Xi'an, Baoji, Hanzhong, Weinan), Gansu (Lanzhou and its surrounding areas), Shanxi (including Yuncheng and Changzhi) and northwestern Xinjiang with surface NH_3 concentrations greater than 8 μg N m^{-3} y^{-1}, which were in agreement with the spatial distributions of the croplands in China (**Fig. S6**). It is not surprising that high surface NH_3 concentrations occurred in eastern

China and Sichuan Basin because the major Chinese croplands are distributed there, as the major source of NH_3 emissions with frequent N fertilizer applications. In addition, N manure is another major source of NH_3 emissions in China, and the percentage of N manure to NH_3 emissions exceeds 50% (Kang et al., 2016). Overall, there was a significant linear correlation between surface NH_3 concentration and N fertilization plus N manure in China (R^2=0.69, p=0.000 in **Fig. 5**). The hotspots also occurred in northwestern Xinjiang surrounding the cropland areas, which may be related to the dry climate that can maintain NH_3 in the gaseous state for a longer time, providing climate conditions for the long distance transmission of NH_3. Recent national measurement work (Pan et al., 2018) also revealed high surface NH_3 concentrations in northwestern Xinjiang, confirming the rationality of the IASI-derived estimates.

In the US, the overall mean surface NH_3 concentrations were 1.52 μg N m^{-3} y^{-1}, with the range of 0.14-10.60 μg N m^{-3}. The surface NH_3 hotspots were generally distributed in the croplands in the central and eastern US (such as Ohio, Illinois, South Dakota, Nebraska, Kansas, Minnesota and North Dakota), as well as in some small areas in western coastal regions (such as California and Washington). In particular, the San Joaquin Valley (SJV) in California (an agricultural land) had the highest surface NH_3 concentrations greater than 4 μg N m^{-3}. The NH_3 source in SJV was from livestock and mineral N fertilizer, which accounted for 74% and 16% of total NH_3 emissions, respectively (Simon et al., 2008). Except the SJV in California, the annual surface NH_3 concentrations in the croplands were mostly within the range of 1-3 μg N m^{-3}, which were much lower than those in eastern China (mostly within the range of 4-10 μg N m^{-3}). Compared with the spatial distribution of N fertilization plus N manure, the hotspots of surface NH_3 concentration can basically reflect the distribution of high N fertilization (R^2=0.37, p=0.000 in **Fig 4 and Fig. 5**).

In Europe, the overall mean surface NH_3 concentrations were 1.8 μg N m^{-3}, with the range of 0.04-9.49 μg N m^{-3}. High surface NH_3 concentrations were distributed widespread in the croplands, especially in the western regions with values greater than 4 μg N m^{-3}, such as Northern Italy (Milan and its surrounding areas), Switzerland,

central and southern Germany, Eastern France (Paris and its surrounding areas) and Poland. According to Emissions Database for Global Atmospheric Research (EDGAR), N manure and N fertilization accounts for 53% and 43% of the NH_3 emissions in western Europe. Overall, there was also a significant linear correlation between surface NH_3 concentration and N fertilization plus N manure (R^2=0.39, p=0.000) in Europe, reflecting the importance of N fertilization on surface NH_3 concentration.

NH_3 is the most abundant alkaline gas in the atmosphere, and has implications to neutralize acidic species (such as H_2SO_4 and HNO_3) to form ammonium salts (such as $(NH_4)_2SO_4$ and NH_4NO_3). Ammonium salts are the important inorganic N components in PM2.5, which can reduce regional visibility and contribute to human disease burden (Van et al., 2015;Yu et al., 2007). Comparing surface NH_3 concentrations with PM2.5 can benefit the understanding of the sources and the mixture of air pollution. The spatial distribution of satellite-derived $PM_{2.5}$ (dust and sea-salt removed) in 2014 (**Fig. S7**) gained from a previous study (Van et al., 2016) was compared with the satellite-derived surface NH_3 concentrations in 2014. On the other hand, NO_2 is also an important precursor of nitrate salts in $PM_{2.5}$. We also included the satellite-derived surface NO_2 concentrations (**Fig. S7**) from a previous study (Geddes et al., 2016) to compare with surface NH_3 and $PM_{2.5}$ concentrations.

The hotspots of surface NH_3 concentrations were highly linked with the hotspots of $PM_{2.5}$. The most severe pollution occurred in the eastern China with annual average $PM_{2.5}$ exceeding 50 μg m^{-3} (much higher than 35 μg m^{-3} as the level 2 annual $PM_{2.5}$ standard set by World Health Organization Air Quality Interim Target-1), and annual average surface NH_3 and NO_2 concentrations greater than 8 μg N m^{-3} and 4 μg N m^{-3}, respectively. A previous study (Xu et al., 2017) reported that the secondary inorganic aerosols of NH_4^+ and NO_3^- can account for 65% of $PM_{2.5}$ based on the measurements in three sites in Beijing. NH_3 and NO_2 are the most important precursors of nitrate salts and ammonium salts, and certainly contribute to the severe pollution in the eastern China. The second severe pollution occurred in the northern India with annual average $PM_{2.5}$ and surface NH_3 concentrations exceeding 40 μg m^{-3} and 4 μg N m^{-3}

respectively (surface NO_2 concentrations less than 1 μg N m^{-3}). The major source of NH_3 in northern India was from agricultural activities and livestock waste management (Warner et al., 2016). The hotspots of surface NH_3 concentrations in the central and eastern US were highly related to the hotspots of $PM_{2.5}$. The annual average $PM_{2.5}$ is less than 10 μg m^{-3} (the first level set by World Health Organization) in the most areas of the US, and only small areas had $PM_{2.5}$ greater than 10 μg m^{-3}. Similarly, in western Europe, the hotspots of high surface NH_3 and NO_2 concentrations (greater than 3 μg N m^{-3}) were consistent with the hotspots of $PM_{2.5}$ (greater than 20 μg m^{-3}).

Seasonal variations of satellite-derived surface NH_3 concentrations

To investigate the seasonal variations of surface NH_3 concentrations, we took the monthly surface NH_3 concentrations in 2014 as a case study (**Fig. 6)**, and analyzed the seasonal surface NH_3 concentrations in hotspot regions including East China (ECH), Sichuan and Chongqing (SCH), Guangdong (GD), Northeast India (NEI), East US (EUS) and West Europe (WEU) (**Fig. 7**).

Seasonal mean IASI-derived surface NH_3 concentrations vary by more than 2 orders of magnitude in hotspot regions, such as the eastern China and eastern US. In China, high surface NH_3 concentrations occurred in spring (March, April and May) and summer (June, July and August) in East China (ECH), Sichuan and Chongqing (SCH), Guangdong (GD). This may be due to two major reasons. First, the timing of the mineral N fertilizer or manure application occurred in summer or spring in the croplands (Paulot et al., 2014). A previous study (Huang et al., 2012) also suggested a summer peak in NH_3 emissions in China, which was consistent with the summer peak in surface NH_3 concentrations. Second, the temperature in warm months is highest in one year, which favors the volatilization of ammonium ($NH_4^+ + OH^- \rightarrow NH_3 + H_2O$). Notably, there is a difference in the seasonal variations of surface NH_3 concentrations between ECH (peaking in June and July) and GD (peaking in March), which was likely related to different crop planting, N fertilization time as well as meteorological factors (Van Damme et al., 2015;Shen et al., 2009;Van Damme et al., 2014a). In the

eastern US (EUS), high surface NH_3 concentrations appeared in warm months (from March to August, **Fig. 7**) with the maximum in May due to higher temperature and emissions in vast croplands, where the agricultural mineral N fertilizers dominate the NH_3 emissions. A previous study also implied a spring peak in NH_3 emissions in the eastern US (Gilliland et al., 2006). Since the spatial patterns of high surface NH_3 concentrations are highly linked with the spatial distributions of croplands, seasonal surface NH_3 concentrations mainly reflects the timing of N fertilizers in the croplands. In western Europe, surface NH_3 concentrations is low in January and February, rising in March and reaching its maximum, keeping high from March to June, then declining from June to December (**Fig. 7**). High NH_3 concentrations appeared from March to June, mainly affected by higher temperature and frequent N fertilization (Van Damme et al., 2014b;Paulot et al., 2014;Van Damme et al., 2015;Whitburn et al., 2015).

To identify the major regions of biomass burning that may affect the spatial distribution of surface NH_3 concentrations, we used the fire products from the moderate resolution imaging spectroradiometer (MODIS) on board the NASA Aqua and Terra. The MODIS climate modeling grid (CMG) global monthly fire location product (level 2, collection 6) developed by the University of Maryland included geographic location of fire, raw count of fire pixels and mean fire radiative power (Giglio et al., 2015). We used the Aqua and Terra CMG fire products on a monthly scale at a spatial resolution of $0.5\,°\,\text{latitude} \times 0.5\,°\,\text{longitude}$ in 2014, and the fire pixel counts were used to identify the hotspot regions of biomass burning. In the major hotspots with frequent fires (mostly in the southern hemisphere), the biomass burning controlled the seasonal surface NH_3 concentrations (**Fig. S8 and Fig. S9**), such as, for instance, Africa north of equator, Africa south of equator and central South America. Apart from the large areas with frequent fires in the southern hemisphere, we also demonstrated the relationship of biomass burning and surface NH_3 concentrations in China, US and Europe, and selected six typical regions in China (CH1 and CH2), US (US1 and US2) and Europe (EU1 and EU2) (**Fig. 8**) to analyze the monthly variations of fire counts and surface NH_3 concentrations.

In China, the first region (CH1) covers the major cropland areas in northern China

including Shandong, Henan and northern Jiangsu Provinces. The fires counts were mainly from the crop straw burning, which contributes large to surface NH_3 concentrations. Both surface NH_3 concentrations and fire counts were found in June likely related to the crop straw burning in this agricultural regions. Notably, despite a decline in fire counts in July, the surface NH_3 concentrations in July did not decrease, probably due to mineral N fertilization for new planted crops (CH1 is typical for spring and summer corn rotations) as well as the high temperature favoring NH_3 volatilization in July. The second region (CH2) is typical for the rice cultivation area in the southern China, where the rice was normally planted in June or July with frequent mineral N fertilization. Thus, the highest surface NH_3 concentrations occurred in June and July. This region is also typical for the winter wheat and summer rice rotations, and the wheat is normally harvested from May to July, which can lead to frequent fire counts there. Despite the more frequent fires in the second region than the first region, the surface NH_3 concentrations in CH2 were much lower than those in CH1. This may be due to the wetter climate and more frequent precipitation events in CH2 than in CH1, resulting in higher scavenging of surface NH_3 concentrations into water.

US1 is a region typical for forest land in the US, and the fire counts are certainly from the forest fires or anthropogenic biomass burning. The monthly variations of surface NH_3 concentrations were consistent with the monthly variations of MODIS fire counts, which peaked in August with high temperature. Instead, US2 is a region typical for mixed agricultural and forest lands, which can be influenced by both potential mineral N fertilization and anthropogenic biomass burning or forest fires. It is clear to see that there is a peak in surface NH_3 concentrations in October resulting from the biomass burning because of the same peak in fire counts in October. However, there is also an apparent peak in surface NH_3 concentrations in May, which may result from the mineral N fertilization in this region. In Europe, the selected two regions of EU1 and EU2 are mainly covered by crops, vegetables as well as forests. For EU2, the monthly variations of surface NH_3 concentrations were consistent with the monthly variations of MODIS fire counts, which peaked in August with high temperature, implying that

the biomass burning may control the seasonal surface NH_3 concentrations. For EU1, there were two peaks of surface NH_3 concentrations including April and August. The August peak can be related to the biomass burning because of the high fire counts, while the April peak may be related to the agricultural fertilizations for the spring crops.

Trends in surface NH_3 concentrations in China, the US and Europe

Time series of nine years' (2008-2016) IASI-derived surface NH_3 concentrations have been fitted using the linear regression method (Geddes et al., 2016;Richter et al., 2005) for all grids on the land. The annual trend (the slope of the linear regression model) is shown in **Fig. 9**. A significant increase rate of surface NH_3 concentrations (>0.2 μg N m^{-3} y^{-1}) appeared in eastern China, and a middle positive trend (0.1-0.2 μg N m^{-3} y^{-1}) occurred in northern Xinjiang, corresponding to its frequent agricultural activities for fertilized crops and dry climate (Warner et al., 2017;Liu et al., 2017b;Xu et al., 2015;Huang et al., 2012). The large increase in eastern China was consistent with the results revealed by AIRS NH_3 data (Warner et al., 2017). The increase of surface NH_3 concentrations in eastern China was consistent with the trend of NH_3 emission estimates by a recent study (Zhang et al., 2017b). China's NH_3 emissions increased significantly from 2008 to 2015, with an increase rate of 1.9% y^{-1}, which was mainly driven by eastern China (Zhang et al., 2017b). Approximately 85% of the inter-annual variations was due to the changes of human activities, and the remaining 15% resulted from air temperature changes. Agricultural activities is the main drive of NH_3 emission increase, of which 43.1% and 36.4% were contributed by livestock manure and fertilizer application (Zhang et al., 2017b). In addition, the increase in surface NH_3 concentrations in eastern China may be also linked with the decreased NH_3 removal due to the decline in acidic gases (NO_2 and SO_2) (Liu et al., 2017a;Xia et al., 2016). NH_3 can react with nitric acid and sulfuric acid to form ammonia sulfate and ammonia nitrate aerosols. The reduction of acidic gases leads to the reduction of NH_3 conversion to ammonia salts in the atmosphere, which may lead to the increase of NH_3 in the atmosphere (Liu et al., 2017a;Li et al., 2017b). China's SO_2 emissions

549 decreased by about 60% in 2008-2016, which led to a 50% decrease in surface SO_2
550 concentrations simulated by WRF model, and then resulted in a 30% increase in
551 surface NH_3 concentrations (Liu et al., 2018).
552 In the US, the NH_3 increase was found in agricultural regions in middle and eastern
553 regions with an annual increase rate of lower than 0.10 μg N m^{-3} y^{-1}, which was
554 consistent with the results of AIRS NH_3 data for a longer time period (2003-2016)
555 (Warner et al., 2017), while we concerned the timespan of 2008-2016 from IASI
556 retrievals. Based on the simulation data of CMAQ model, it is also found that NH_3
557 increased significantly in the eastern US from 1990 to 2010, which is inconsistent
558 with the significant downward trend of NO_x emissions (Zhang et al., 2018). This
559 inconsistency between NH_3 and NO_x trends in the US was mainly due to different
560 emission control policies. Over the past two decades, due to the implementation of
561 effective regulations and emission reduction measures for NO_x, the NO_x emission in
562 the US decreased by nearly 41% between 1990 and 2010 (Hand et al., 2014).
563 However, this NH_3 increase in eastern US is likely due to the lack of NH_3 emission
564 control policy as well as the decreased NH_3 removal due to the decline in acidic gases
565 (NO_2 and SO_2) (Warner et al., 2017;Li et al., 2016). As NH_3 is an uncontrolled gas in
566 the US, NH_3 emissions have continuously increased since 1990, and by 2003 NH_3
567 emissions had begun to dominate the inorganic N emissions (NO_x plus NH_3) (Zhang
568 et al., 2018). For the western Europe, the trend was close to 0 in most regions
569 although we can observe the NH_3 increase in many points with small positive trend of
570 lower than 0.1 μg N m^{-3} y^{-1}. Compared with the trend of surface NH_3 concentrations
571 in China and the US, the change of surface NH_3 concentrations in western Europe is
572 more stable, which may be related to the mature NH_3 reduction policies and measures
573 in Europe. Since 1990, Europe has implemented a series of agricultural NH_3 emission
574 reduction measures, and NH_3 emissions decreased by about 29% between 1990 and
575 2009 (Tørseth et al., 2012b). For example, due to serious N eutrophication, the
576 Netherlands has taken measures to reduce NH_3 emissions by nearly two times in the
577 past 20 years, while maintaining a high level of food production (Dentener et al.,
578 2006). The N fertilizer use in Europe has decreased widespread according to the data

from the World Bank (http://data.worldbank.org/indicator/AG.CON.FERT.ZS) with an annual decrease of -8.84~-17.7 kg ha^{-1} y^{-1} in fertilizer use in Europe (Warner et al., 2017).

Conclusions

The IASI-derived global surface NH_3 concentrations during 2008-2016 were inferred based on IASI NH_3 column measurements as well as NH_3 vertical profiles from the GEOS-Chem in this study. Global NH_3 vertical profiles on the land from the GEOS-Chem can be well modelled by the Gaussian function between 60 °N and 55 °S with R^2 higher than 0.90. The IASI-derived surface NH_3 concentrations were compared to the in situ measurements over China, the US and Europe. One of the major findings is that a relatively high predictive power for annual surface NH_3 concentrations was achieved through converting IASI NH_3 columns using modelled NH_3 vertical profiles, and the validation with the ground-based measurements shows that IASI-derived surface NH_3 concentrations had higher accuracy in China than the US and Europe. High surface NH_3 concentrations were found in the croplands in China, US and Europe, and surface NH_3 concentrations in the croplands in China were approximately double than those in the US and Europe. Seasonal mean IASI-derived surface NH_3 concentrations vary by more than 2 orders of magnitude in hotspot regions, such as the eastern China and eastern US. The linear trend analysis shows that a significant positive increase rate of above 0.2 μg N m^{-3} y^{-1} appeared in the eastern China during 2008-2016, and a middle increase trend (0.1-0.2 μg N m^{-3} y^{-1}) occurred in northern Xinjiang Province. In the US, the NH_3 increase was found in agricultural regions in middle and eastern regions with an annual increase rate of lower than 0.10 μg N m^{-3} y^{-1}.

Author contributions

LL and XZ designed the research; WX and XL's group conducted the field work in China; LL prepared IASI NH_3 products; LL and AW conducted model simulations; LL, WX, LZ, XW and ZW performed the data analysis and prepared the figures; LL,

AW and XZ wrote the paper, and all coauthors contribute to the revision.

Acknowledgements

We acknowledge the free use of IASI NH_3 data from the Atmospheric Spectroscopy Group at Universit élibre de Bruxelles (ULB). We thank Dr. Jeffrrey A. Geddes for the help of using the GEOS-Chem in this work. This study is supported by the National Natural Science Foundation of China (No. 41471343, 41425007, 41101315 and 41705130) and Doctoral Research Innovation Fund (2016CL07) as well as the Chinese National Programs on Heavy Air Pollution Mechanisms and Enhanced Prevention Measures (Project No. 8 in the 2nd Special Program).

Data availability

The IASI NH_3 satellite datasets are available at: http://iasi.aeris-data.fr/NH3. The ground-based NH_3 mesurements in Chinese Nationwide Nitrogen Deposition Monitoring Network (NNDMN) can be requested from Prof. Xuejun Liu in China Agricutural University. The ground-based NH_3 measurements from the AMoN-US can be downloaded from the website: http://nadp.sws.uiuc.edu/AMoN/. The ground-based NH_3 measurements from the EMEP network can be gained from https://www.nilu.no/projects/ccc/emepdata.html. The IASI-derived surface NH_3 used in this study are available from the corresponding author upon request.

Competing interests

The authors declare that they have no conflict of interest.

Reference

Amos, H. M., Jacob, D. J., Holmes, C. D., Fisher, J. A., Wang, Q., Yantosca, R. M., Corbitt, E. S., Galarneau, E., Rutter, A. P., and Gustin, M. S.: Gas-particle partitioning of atmospheric Hg(II) and its effect on global mercury deposition, Atmospheric Chemistry & Physics, 11, 29441-29477, 2012.

Basto, S., Thompson, K., Phoenix, G., Sloan, V., Leake, J., and Rees, M.: Long-term

633 nitrogen deposition depletes grassland seed banks, Nature Communication, 6, 1-6,
634 10.1038/ncomms7185, 2015.
635 Bobrutzki, K. V., Braban, C. F., Famulari, D., Jones, S. K., Blackall, T., Smith, T. E.
636 L., Blom, M., Coe, H., Gallagher, M., and Ghalaieny, M.: Field inter-comparison of
637 eleven atmospheric ammonia measurement techniques, Atmospheric Measurement
638 Techniques,3,1(2010-01-27), 2, 91-112, 2010.
639 Crippa, M., Guizzardi, D., Muntean, M., Schaaf, E., Dentener, F., van Aardenne, J. A.,
640 Monni, S., Doering, U., Olivier, J. G. J., Pagliari, V., and Janssens-Maenhout, G.:
641 Gridded emissions of air pollutants for the period 1970–2012 within EDGAR v4.3.2,
642 Earth Syst. Sci. Data, 10, 1987-2013, 10.5194/essd-10-1987-2018, 2018.
643 Dammers, E., Palm, M., Van Damme, M., Vigouroux, C., Smale, D., Conway, S.,
644 Toon, G. C., Jones, N., Nussbaumer, E., Warneke, T., Petri, C., Clarisse, L., Clerbaux,
645 C., Hermans, C., Lutsch, E., Strong, K., Hannigan, J. W., Nakajima, H., Morino, I.,
646 Herrera, B., Stremme, W., Grutter, M., Schaap, M., Wichink Kruit, R. J., Notholt, J.,
647 Coheur, P. F., and Erisman, J. W.: An evaluation of IASI-NH_3 with ground-based
648 Fourier transform infrared spectroscopy measurements, Atmospheric Chemistry and
649 Physics, 16, 10351-10368, 10.5194/acp-16-10351-2016, 2016.
650 Dentener, F., Drevet, J., Lamarque, J., Bey, I., Eickhout, B., Fiore, A., Hauglustaine,
651 D., Horowitz, L., Krol, M., and Kulshrestha, U.: Nitrogen and sulfur deposition on
652 regional and global scales: a multimodel evaluation, Global Biogeochemical Cycles,
653 20, 2006.
654 Eerden, L. J. M. V. D.: Toxicity of ammonia to plants, Agriculture & Environment, 7,
655 223-235, 1982.
656 Fountoukis, C., and Nenes, A.: ISORROPIA II: a computationally efficient
657 thermodynamic equilibrium model for aerosols, Atmospheric Chemistry and Physics,
658 7, 4639-4659, 2007.
659 Geddes, J. A., Martin, R. V., Boys, B. L., and van Donkelaar, A.: Long-term trends
660 worldwide in ambient NO_2 concentrations inferred from satellite observations,
661 Environmental Health Perspectives, 124, 281, 2016.
662 Geng, G., Zhang, Q., Martin, R. V., Donkelaar, A. V., Huo, H., Che, H., Lin, J., and

He, K.: Estimating long-term PM 2.5 concentrations in China using satellite-based aerosol optical depth and a chemical transport model, Remote Sensing of Environment, 166, 262-270, 2015.

Giglio, L., Randerson, J. T., and van der Werf, G. R.: Analysis of daily, monthly, and annual burned area using the fourth-generation global fire emissions database (GFED4), Journal of Geophysical Research: Biogeosciences, 118, 317-328, 10.1002/jgrg.20042, 2013.

Giglio, L., Csiszar, I., and Justice, C. O.: Global distribution and seasonality of active fires as observed with the Terra and Aqua Moderate Resolution Imaging Spectroradiometer (MODIS) sensors, Journal of Geophysical Research Biogeosciences, 111, 17-23, 2015.

Gilliland, A. B., Wyat Appel, K., Pinder, R. W., and Dennis, R. L.: Seasonal NH_3 emissions for the continental united states: Inverse model estimation and evaluation, Atmospheric Environment, 40, 4986-4998, https://doi.org/10.1016/j.atmosenv.2005.12.066, 2006.

Graaf, S. C. v. d., Dammers, E., Schaap, M., and Erisman, J. W.: How are NH_3 dry deposition estimates affected by combining the LOTOS-EUROS model with IASI-NH3 satellite observations?, Atmospheric Chemistry and Physics, 18, 13173-13196, https://doi.org/10.5194/acp-2018-133, 2018.

Hand, J. L., Schichtel, B. A., Malm, W. C., Copeland, S., Molenar, J. V., Frank, N., and Pitchford, M.: Widespread reductions in haze across the United States from the early 1990s through 2011, Atmospheric Environment, 94, 671-679, 2014.

Huang, X., Song, Y., Li, M., Li, J., Huo, Q., Cai, X., Zhu, T., Hu, M., and Zhang, H.: A high resolution ammonia emission inventory in China, Global Biogeochemical Cycles, 26, 1-14, 2012.

Janssens-Maenhout, G., Crippa, M., Guizzardi, D., Dentener, F., Muntean, M., Pouliot, G., Keating, T., Zhang, Q., Kurokawa, J., Wankmüller, R., Denier van der Gon, H., Kuenen, J. J. P., Klimont, Z., Frost, G., Darras, S., Koffi, B., and Li, M.: HTAP_v2.2: a mosaic of regional and global emission grid maps for 2008 and 2010 to study hemispheric transport of air pollution, Atmos. Chem. Phys., 15, 11411-11432,

693 10.5194/acp-15-11411-2015, 2015.
694 Kang, Y., Liu, M., Song, Y., Huang, X., Yao, H., Cai, X., Zhang, H., Kang, L., Liu, X.,
695 Yan, X., He, H., Zhang, Q., Shao, M., and Zhu, T.: High-resolution ammonia
696 emissions inventories in China from 1980 to 2012, Atmospheric Chemistry and
697 Physics, 16, 2043-2058, 10.5194/acp-16-2043-2016, 2016.
698 Kharol, S. K., Shephard, M. W., McLinden, C. A., Zhang, L., Sioris, C. E., O'Brien, J.
699 M., Vet, R., Cady-Pereira, K. E., Hare, E., Siemons, J., and Krotkov, N. A.: Dry
700 Deposition of Reactive Nitrogen From Satellite Observations of Ammonia and
701 Nitrogen Dioxide Over North America, Geophysical Research Letters, 45, 1157-1166,
702 10.1002/2017GL075832, 2018.
703 Kim, T. W., Lee, K., Duce, R., and Liss, P.: Impact of atmospheric nitrogen deposition
704 on phytoplankton productivity in the South China Sea, Geophysical Research Letters,
705 41, 3156–3162, 2014.
706 Lamarque, J. F., Kiehl, J., Brasseur, G., Butler, T., Cameron‐Smith, P., Collins, W.,
707 Collins, W., Granier, C., Hauglustaine, D., and Hess, P.: Assessing future nitrogen
708 deposition and carbon cycle feedback using a multimodel approach: Analysis of
709 nitrogen deposition, Journal of Geophysical Research: Atmospheres (1984–2012), 110,
710 2005.
711 Lamsal, L. N., Martin, R. V., van Donkelaar, A., Steinbacher, M., Celarier, E. A.,
712 Bucsela, E., Dunlea, E. J., and Pinto, J. P.: Ground-level nitrogen dioxide
713 concentrations inferred from the satellite-borne Ozone Monitoring Instrument, Journal
714 of Geophysical Research: Atmospheres, 113, 1-15, 10.1029/2007JD009235, 2008.
715 Lamsal, L. N., Martin, R. V., Parrish, D. D., and Krotkov, N. A.: Scaling relationship
716 for NO_2 pollution and urban population size: a satellite perspective, Environmental
717 Science & Technology, 47, 7855-7861, 2013.
718 Larssen, T., Duan, L., and Mulder, J.: Deposition and leaching of sulfur, nitrogen and
719 calcium in four forested catchments in China: implications for acidification,
720 Environmental science & technology, 45, 1192-1198, 2011.
721 Lenhart, L., and Friedrich, R.: European emission data with high temporal and spatial
722 resolution, Water Air & Soil Pollution, 85, 1897-1902, 1995.

723 Levine, J. S., Augustsson, T. R., and Hoell, J. M.: The vertical distribution of
724 tropospheric ammonia, Geophysical Research Letters, 7, 317-320,
725 10.1029/GL007i005p00317, 1980.
726 Li, M., Zhang, Q., Kurokawa, J., Woo, J. H., He, K., Lu, Z., Ohara, T., Song, Y.,
727 Streets, D. G., and Carmichael, G. R.: MIX: a mosaic Asian anthropogenic emission
728 inventory under the international collaboration framework of the MICS-Asia and
729 HTAP, Atmospheric Chemistry & Physics, 17, 34813-34869, 2017a.
730 Li, Y., Schwandner, F. M., Sewell, H. J., Zivkovich, A., Tigges, M., Raja, S., Holcomb,
731 S., Molenar, J. V., Sherman, L., and Archuleta, C.: Observations of ammonia, nitric
732 acid, and fine particles in a rural gas production region, Atmospheric Environment, 83,
733 80-89, 2014.
734 Li, Y., Schichtel, B. A., Walker, J. T., Schwede, D. B., Chen, X., Lehmann, C. M.,
735 Puchalski, M. A., Gay, D. A., and Collett, J. L.: Increasing importance of deposition of
736 reduced nitrogen in the United States, Proceedings of the National Academy of
737 Sciences, 113, 5874-5879, 2016.
738 Li, Y., Thompson, T. M., Damme, M. V., Chen, X., Benedict, K. B., Shao, Y., Day, D.,
739 Boris, A., Sullivan, A. P., and Ham, J.: Temporal and Spatial Variability of Ammonia
740 in Urban and Agricultural Regions of Northern Colorado, United States, Atmospheric
741 Chemistry & Physics, 17, 1-50, 2017b.
742 Lin, J. T., Martin, R. V., Boersma, K. F., Sneep, M., Stammes, P., Spurr, R., Wang, P.,
743 Van Roozendael, M., Clémer, K., and Irie, H.: Retrieving tropospheric nitrogen
744 dioxide from the Ozone Monitoring Instrument: effects of aerosols, surface
745 reflectance anisotropy, and vertical profile of nitrogen dioxide, Atmospheric
746 Chemistry and Physics, 14, 1441-1461, 10.5194/acp-14-1441-2014, 2014.
747 Liu, H., Jacob, D. J., Bey, I., and Yantosca, R. M.: Constraints from 210Pb and 7Be on
748 wet deposition and transport in a global three-dimensional chemical tracer model
749 driven by assimilated meteorological fields, Journal of Geophysical Research:
750 Atmospheres, 106, 12109-12128, 10.1029/2000JD900839, 2001.
751 Liu, L., Zhang, X., Xu, W., Liu, X., Li, Y., Lu, X., Zhang, Y., and Zhang, W.:
752 Temporal characteristics of atmospheric ammonia and nitrogen dioxide over China

based on emission data, satellite observations and atmospheric transport modeling since 1980, Atmospheric Chemistry & Physics, 17, 1-32, 2017a.

Liu, L., Zhang, X., Xu, W., Liu, X., Lu, X., Wang, S., Zhang, W., and Zhao, L.: Ground Ammonia Concentrations over China Derived from Satellite and Atmospheric Transport Modeling, Remote Sensing, 9, 467, 2017b.

Liu, L., Zhang, X., Zhang, Y., Xu, W., Liu, X., Zhang, X., Feng, J., Chen, X., Zhang, Y., Lu, X., Wang, S., Zhang, W., and Zhao, L.: Dry Particulate Nitrate Deposition in China, Environmental Science & Technology, 51, 5572-5581, 10.1021/acs.est.7b00898, 2017c.

Liu, M., Huang, X., Song, Y., Xu, T., Wang, S., Wu, Z., Hu, M., Zhang, L., Zhang, Q., Pan, Y., Liu, X., and Zhu, T.: Rapid SO_2 emission reductions significantly increase tropospheric ammonia concentrations over the North China Plain, Atmospheric Chemistry and Physics, 18, 17933-17943, 10.5194/acp-18-17933-2018, 2018.

Mao, J., Paulot, F., Jacob, D. J., Cohen, R. C., Crounse, J. D., Wennberg, P. O., Keller, C. A., Hudman, R. C., Barkley, M. P., and Horowitz, L. W.: Ozone and organic nitrates over the eastern United States: Sensitivity to isoprene chemistry, Journal of Geophysical Research Atmospheres, 118, 11-11,268, 2013.

Nowlan, C., Martin, R., Philip, S., Lamsal, L., Krotkov, N., Marais, E., Wang, S., and Zhang, Q.: Global dry deposition of nitrogen dioxide and sulfur dioxide inferred from space-based measurements, Global Biogeochemical Cycles, 28, 1025-1043, 2014.

Pan, Y., Tian, S., Zhao, Y., Zhang, L., Zhu, X., Gao, J., Huang, W., Zhou, Y., Song, Y., and Zhang, Q.: Identifying ammonia hotspots in China using a national observation network, Environmental Science & Technology, 2018.

Paulot, F., Jacob, D. J., Pinder, R. W., Bash, J. O., Travis, K., and Henze, D. K.: Ammonia emissions in the United States, European Union, and China derived by high-resolution inversion of ammonium wet deposition data: Interpretation with a new agricultural emissions inventory (MASAGE_NH_3), Journal of Geophysical Research: Atmospheres, 119, 4343-4364, 10.1002/2013JD021130, 2014.

Potter, P., Ramankutty, N., Bennett, E. M., and Donner, S. D.: Characterizing the Spatial Patterns of Global Fertilizer Application and Manure Production, Earth

783 Interactions, 14, 1-22, 10.1175/2009EI288.1, 2010.
784 Preston, K. E., Jones, R. L., and Roscoe, H. K.: Retrieval of NO_2 vertical profiles
785 from ground-based UV-visible measurements: Method and validation, Journal of
786 Geophysical Research: Atmospheres, 102, 19089-19097, doi:10.1029/97JD00603,
787 1997.
788 Puchalski, M. A., Sather, M. E., Walker, J. T., Lehmann, C. M. B., Gay, D. A.,
789 Johnson, M., and Robarge, W. P.: Passive ammonia monitoring in the United States:
790 comparing three different sampling devices, Journal of Environmental Monitoring, 13,
791 3156, 2011.
792 Pye, H. O. T., Liao, H., Wu, S., Mickley, L. J., Jacob, D. J., Henze, D. K., and
793 Seinfeld, J. H.: Effect of changes in climate and emissions on future
794 sulfate-nitrate-ammonium aerosol levels in the United States, Journal of Geophysical
795 Research: Atmospheres, 114, 10.1029/2008jd010701, 2009.
796 Reay, D. S., Dentener, F., Smith, P., Grace, J., and Feely, R. A.: Global nitrogen
797 deposition and carbon sinks, Nature Geoscience, 1, 430-437, 2008.
798 Richter, A., Burrows, J. P., Nüß, H., Granier, C., and Niemeier, U.: Increase in
799 tropospheric nitrogen dioxide over China observed from space, Nature, 437, 129-132,
800 2005.
801 Rozanov, A., Bovensmann, H., Bracher, A., Hrechanyy, S., Rozanov, V., Sinnhuber,
802 M., Stroh, F., and Burrows, J. P.: NO2 and BrO vertical profile retrieval from
803 SCIAMACHY limb measurements: Sensitivity studies, Advances in Space Research,
804 36, 846-854, https://doi.org/10.1016/j.asr.2005.03.013, 2005.
805 Schaap, M., van Loon, M., ten Brink, H. M., Dentener, F. J., and Builtjes, P. J. H.:
806 Secondary inorganic aerosol simulations for Europe with special attention to nitrate,
807 Atmos. Chem. Phys., 4, 857-874, 10.5194/acp-4-857-2004, 2004.
808 Schiferl, L. D., Heald, C. L., Nowak, J. B., Holloway, J. S., Neuman, J. A., Bahreini,
809 R., Pollack, I. B., Ryerson, T. B., Wiedinmyer, C., and Murphy, J. G.: An investigation
810 of ammonia and inorganic particulate matter in California during the CalNex
811 campaign, Journal of Geophysical Research: Atmospheres, 119, 1883-1902, 2014.
812 Schiferl, L. D., Heald, C. L., Van Damme, M., Pierrefrancois, C., and Clerbaux, C.:

Interannual Variability of Ammonia Concentrations over the United States: Sources and Implications for Inorganic Particulate Matter, Atmospheric Chemistry & Physics, 1-42, 2015.

Shen, J. L., Tang, A. H., Liu, X. J., Fangmeier, A., Goulding, K. T. W., and Zhang, F. S.: High concentrations and dry deposition of reactive nitrogen species at two sites in the North China Plain, Environmental Pollution, 157, 3106-3113, http://dx.doi.org/10.1016/j.envpol.2009.05.016, 2009.

Shephard, M., and Cady-Pereira, K.: Cross-track Infrared Sounder (CrIS) satellite observations of tropospheric ammonia, Atmospheric Measurement Techniques, 8, 1323-1336, 2015.

Shephard, M. W., Cady-Pereira, K. E., Luo, M., Henze, D. K., Pinder, R. W., Walker, J. T., Rinsland, C. P., Bash, J. O., Zhu, L., Payne, V. H., and Clarisse, L.: TES ammonia retrieval strategy and global observations of the spatial and seasonal variability of ammonia, Atmos. Chem. Phys., 11, 10743-10763, 10.5194/acp-11-10743-2011, 2011.

Sheppard, L. J., Leith, I. D., Crossley, A., Dijk, N. V., Fowler, D., Sutton, M. A., and Woods, C.: Stress responses of Calluna vulgaris to reduced and oxidised N applied under 'real world conditions', Environmental Pollution, 154, 404-413, 2008.

Simon, H., Allen, D. T., and Wittig, A. E.: Fine particulate matter emissions inventories: comparisons of emissions estimates with observations from recent field programs, Journal of the Air & Waste Management Association, 58, 320-343, 2008.

Sutton, M. A., Tang, Y. S., Miners, B., and Fowler, D.: A New Diffusion Denuder System for Long-Term, Regional Monitoring of Atmospheric Ammonia and Ammonium, Water Air & Soil Pollution Focus, 1, 145-156, 2001.

Tørseth, K., Aas, W., Breivik, K., Fjæraa, A. M., Fiebig, M., Hjellbrekke, A. G., Lund Myhre, C., Solberg, S., and Yttri, K. E.: Introduction to the European Monitoring and Evaluation Programme (EMEP) and observed atmospheric composition change during 1972–2009, Atmos. Chem. Phys., 12, 5447-5481, 10.5194/acp-12-5447-2012, 2012a.

Tørseth, K., Aas, W., Breivik, K., Fjæraa, A. M., Fiebig, M., Hjellbrekke, A. G., Lund Myhre, C., Solberg, S., and Yttri, K. E.: Introduction to the European Monitoring and

Evaluation Programme (EMEP) and observed atmospheric composition change during 1972-2009, Atmospheric Chemistry and Physics, 12, 5447-5481, 2012b.

Tevlin, A. G., Li, Y., Collett, J. L., Mcduffie, E. E., Fischer, E. V., and Murphy, J. G.: Tall Tower Vertical Profiles and Diurnal Trends of Ammonia in the Colorado Front Range, Journal of Geophysical Research Atmospheres, 122, 2017.

Van, D. A., Martin, R. V., Spurr, R. J., and Burnett, R. T.: High-Resolution Satellite-Derived PM2.5 from Optimal Estimation and Geographically Weighted Regression over North America, Environmental Science & Technology, 49, 10482-10491, 2015.

Van, D. A., Martin, R. V., Brauer, M., Hsu, N. C., Kahn, R. A., Levy, R. C., Lyapustin, A., Sayer, A. M., and Winker, D. M.: Global Estimates of Fine Particulate Matter using a Combined Geophysical-Statistical Method with Information from Satellites, Models, and Monitors, Environmental Science & Technology, 50, 3762, 2016.

Van Damme, M., Clarisse, L., Dammers, E., Liu, X., Nowak, J., Clerbaux, C., Flechard, C., Galy-Lacaux, C., Xu, W., and Neuman, J.: Towards validation of ammonia (NH_3) measurements from the IASI satellite, Atmospheric Measurement Techniques, 7, 12125-12172, 2014a.

Van Damme, M., Clarisse, L., Heald, C., Hurtmans, D., Ngadi, Y., Clerbaux, C., Dolman, A., Erisman, J. W., and Coheur, P.-F.: Global distributions, time series and error characterization of atmospheric ammonia (NH_3) from IASI satellite observations, Atmospheric Chemistry and Physics, 14, 2905-2922, 2014b.

Van Damme, M., Wichink Kruit, R., Schaap, M., Clarisse, L., Clerbaux, C., Coheur, P. F., Dammers, E., Dolman, A., and Erisman, J.: Evaluating 4 years of atmospheric ammonia (NH_3) over Europe using IASI satellite observations and LOTOS-EUROS model results, Journal of Geophysical Research: Atmospheres, 119, 9549-9566, 2014c.

Van Damme, M., Erisman, J. W., Clarisse, L., Dammers, E., Whitburn, S., Clerbaux, C., Dolman, A. J., and Coheur, P. F.: Worldwide spatiotemporal atmospheric ammonia (NH_3) columns variability revealed by satellite, Geophysical Research Letters, 42, 8660-8668, 2015.

Van Damme, M., Whitburn, S., Clarisse, L., Clerbaux, C., Hurtmans, D., and Coheur, P. F.: Version2 of the IASI NH_3 neural network retrieval algorithm: near-real-time and reanalysed datasets, Atmospheric Measurement Techniques, 10, 1-14, 2017.

Van Damme, M., Clarisse, L., Whitburn, S., Hadji-Lazaro, J., Hurtmans, D., Clerbaux, C., and Coheur, P.-F.: Industrial and agricultural ammonia point sources exposed, Nature, 564, 99-103, 10.1038/s41586-018-0747-1, 2018.

Wang, Q., Jacob, D. J., Fisher, J. A., and Mao, J.: Sources of carbonaceous aerosols and deposited black carbon in the Arctic in winter-spring: implications for radiative forcing, Atmospheric Chemistry and Physics Discussions, 11, 19395-19442, 2011.

Wang, Y., Logan, J. A., and Jacob, D. J.: Global simulation of tropospheric O 3 -NO x -hydrocarbon chemistry: 2. Model evaluation and global ozone budget, Journal of Geophysical Research Atmospheres, 103, 10727-10755, 1998.

Warner, J. X., Wei, Z., Strow, L. L., Dickerson, R. R., and Nowak, J. B.: The global tropospheric ammonia distribution as seen in the 13-year AIRS measurement record, Atmospheric Chemistry and Physics, 16, 5467-5479, 2016.

Warner, J. X., Dickerson, R. R., Wei, Z., Strow, L. L., Wang, Y., and Liang, Q.: Increased atmospheric ammonia over the world's major agricultural areas detected from space, Geophysical Research Letters, 10.1002/2016GL072305, 2017.

Wei, J., Li, Z., Peng, Y., and Sun, L.: MODIS Collection 6.1 aerosol optical depth products over land and ocean: validation and comparison, Atmospheric Environment, 201, 1-13, 2019.

Wesely, M.: Parameterization of surface resistances to gaseous dry deposition in regional-scale numerical models, Atmospheric Environment, 23, 1293-1304, 1989.

Whitburn, S., Van Damme, M., Kaiser, J. W., van der Werf, G. R., Turquety, S., Hurtmans, D., Clarisse, L., Clerbaux, C., and Coheur, P. F.: Ammonia emissions in tropical biomass burning regions: Comparison between satellite-derived emissions and bottom-up fire inventories, Atmospheric Environment, 121, 42-54, https://doi.org/10.1016/j.atmosenv.2015.03.015, 2015.

Whitburn, S., Van Damme, M., Clarisse, L., Bauduin, S., Heald, C. L., Hadji-Lazaro, J., Hurtmans, D., Zondlo, M. A., Clerbaux, C., and Coheur, P. F.: A flexible and robust

neural network IASI-NH_3 retrieval algorithm, Journal of Geophysical Research: Atmospheres, 121, 6581-6599, 10.1002/2016JD024828, 2016.

Xia, Y., Zhao, Y., and Nielsen, C. P.: Benefits of China's efforts in gaseous pollutant control indicated by the bottom-up emissions and satellite observations 2000–2014, Atmospheric Environment, 136, 43-53, http://dx.doi.org/10.1016/j.atmosenv.2016.04.013, 2016.

Xu, W., Luo, X. S., Pan, Y. P., Zhang, L., Tang, A. H., Shen, J. L., Zhang, Y., Li, K. H., Wu, Q. H., Yang, D. W., Zhang, Y. Y., Xue, J., Li, W. Q., Li, Q. Q., Tang, L., Lv, S. H., Liang, T., Tong, Y. A., Liu, P., Zhang, Q., Xiong, Z. Q., Shi, X. J., Wu, L. H., Shi, W. Q., Tian, K., Zhong, X. H., Shi, K., Tang, Q. Y., Zhang, L. J., Huang, J. L., He, C. E., Kuang, F. H., Zhu, B., Liu, H., Jin, X., Xin, Y. J., SHi, X. K., Du, E. Z., Dore, A. J., Tang, S., Collett Jr, J. L., Goulding, K., Sun, Y. X., Ren, J., Zhang, F. S., and Liu, X. J.: Quantifying atmospheric nitrogen deposition through a nationwide monitoring network across China, Atmospheric Chemistry and Physics, 15, 12345-12360, 2015.

Xu, W., Song, W., Zhang, Y., Liu, X., Zhang, L., Zhao, Y., Liu, D., Tang, A., Yang, D., and Wang, D.: Air quality improvement in a megacity: implications from 2015 Beijing Parade Blue pollution control actions, Atmospheric Chemistry and Physics, 17, 31-46, 2017.

Yu, Y., Xu, M., Yao, H., Yu, D., Qiao, Y., Sui, J., Liu, X., and Cao, Q.: Char characteristics and particulate matter formation during Chinese bituminous coal combustion, Proceedings of the Combustion Institute, 31, 1947-1954, http://dx.doi.org/10.1016/j.proci.2006.07.116, 2007.

Zhang, L., Gong, S., Padro, J., and Barrie, L.: A size-segregated particle dry deposition scheme for an atmospheric aerosol module, Atmospheric Environment, 35, 549-560, http://dx.doi.org/10.1016/S1352-2310(00)00326-5, 2001.

Zhang, L., Chen, Y., Zhao, Y., Henze, D. K., Zhu, L., Song, Y., Paulot, F., Liu, X., Pan, Y., and Huang, B.: Agricultural ammonia emissions in China: reconciling bottom-up and top-down estimates, Atmospheric Chemistry & Physics, 18, 1-36, 2017a.

Zhang, X., Wu, Y., Liu, X., Reis, S., Jin, J., Dragosits, U., Van Damme, M., Clarisse, L., Whitburn, S., Coheur, P.-F., and Gu, B.: Ammonia Emissions May Be

933 Substantially Underestimated in China, Environmental Science & Technology, 51,
934 12089-12096, 10.1021/acs.est.7b02171, 2017b.
935 Zhang, Y., Mathur, R., Bash, J. O., Hogrefe, C., Xing, J., and Roselle, S. J.: Long-term
936 trends in total inorganic nitrogen and sulfur deposition in the U.S. from 1990 to 2010,
937 Atmospheric Chemistry & Physics, 1-27, 2018.
938 Zhu, L., Henze, D. K., Cady-Pereira, K. E., Shephard, M. W., Luo, M., Pinder, R. W.,
939 Bash, J. O., and Jeong, G. R.: Constraining U.S. ammonia emissions using TES
940 remote sensing observations and the GEOS‐Chem adjoint model, Journal of
941 Geophysical Research Atmospheres, 118, 3355-3368, 2013.
942
943

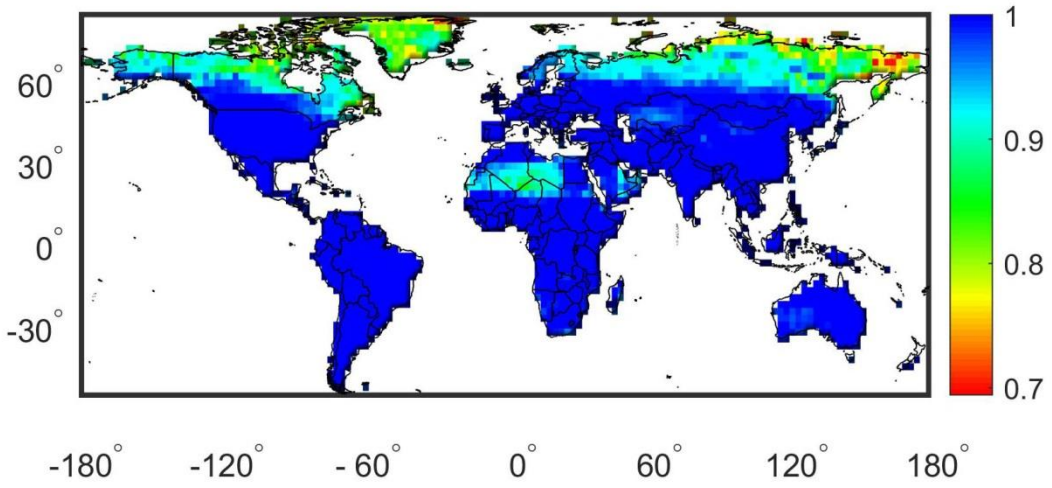

Fig. 1 R^2 of Gaussian fit for NH_3 vertical profiles.

948

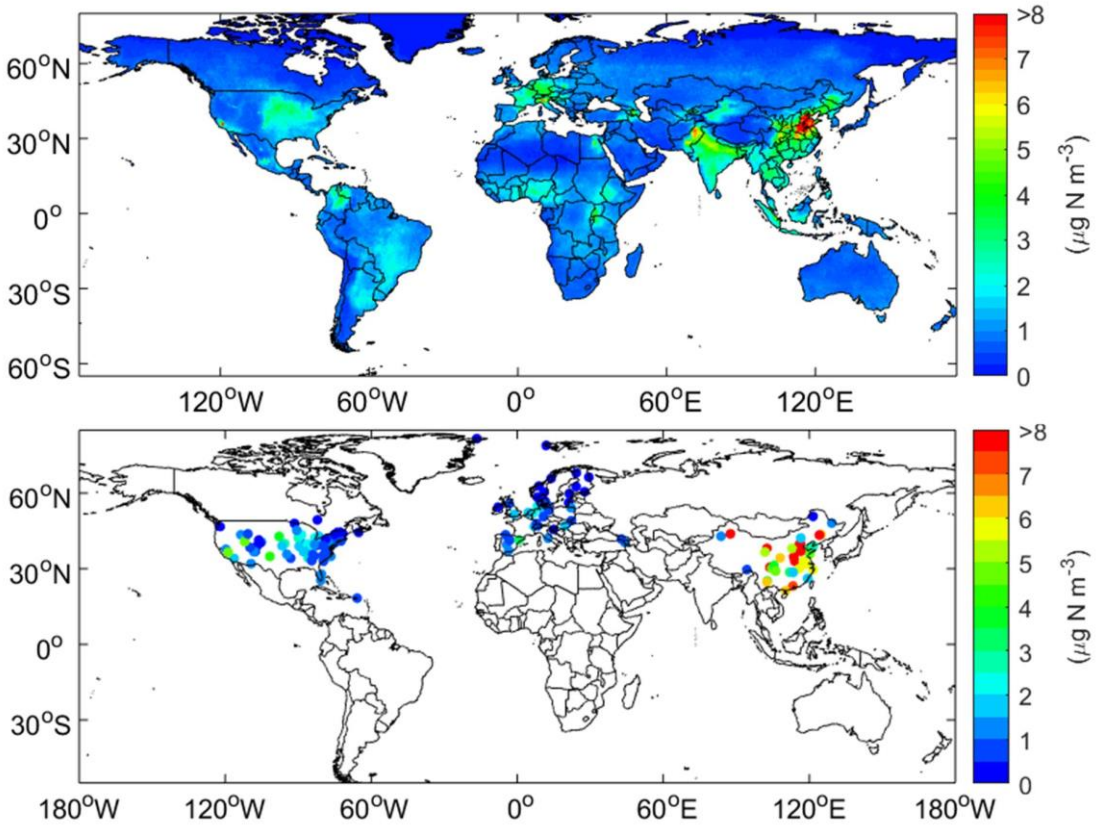

949

950 **Fig. 2** Spatial distribution of satellite-derived and measured surface NH_3 concentrations in 2014.

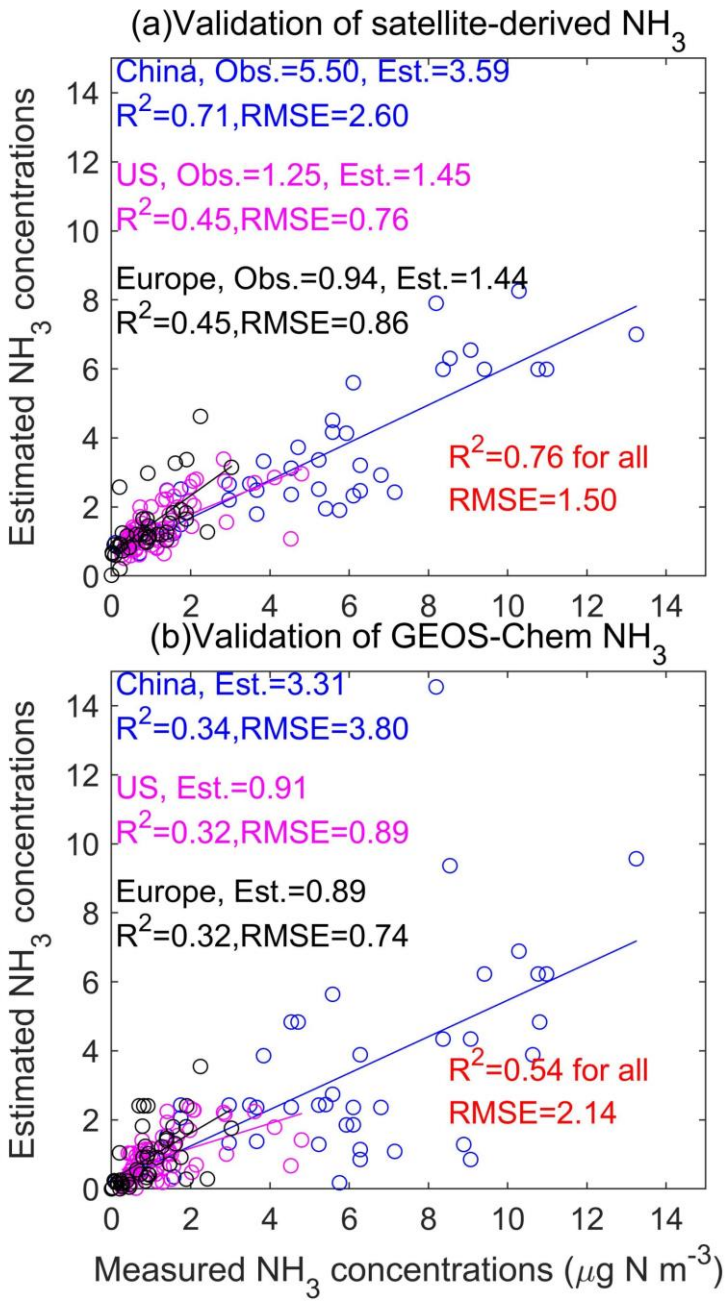

951

952 **Fig. 3** Comparison of satellite-derived and GEOS-Chem modelled surface NH_3 concentrations with
953 measured concentrations in China, US and Europe.

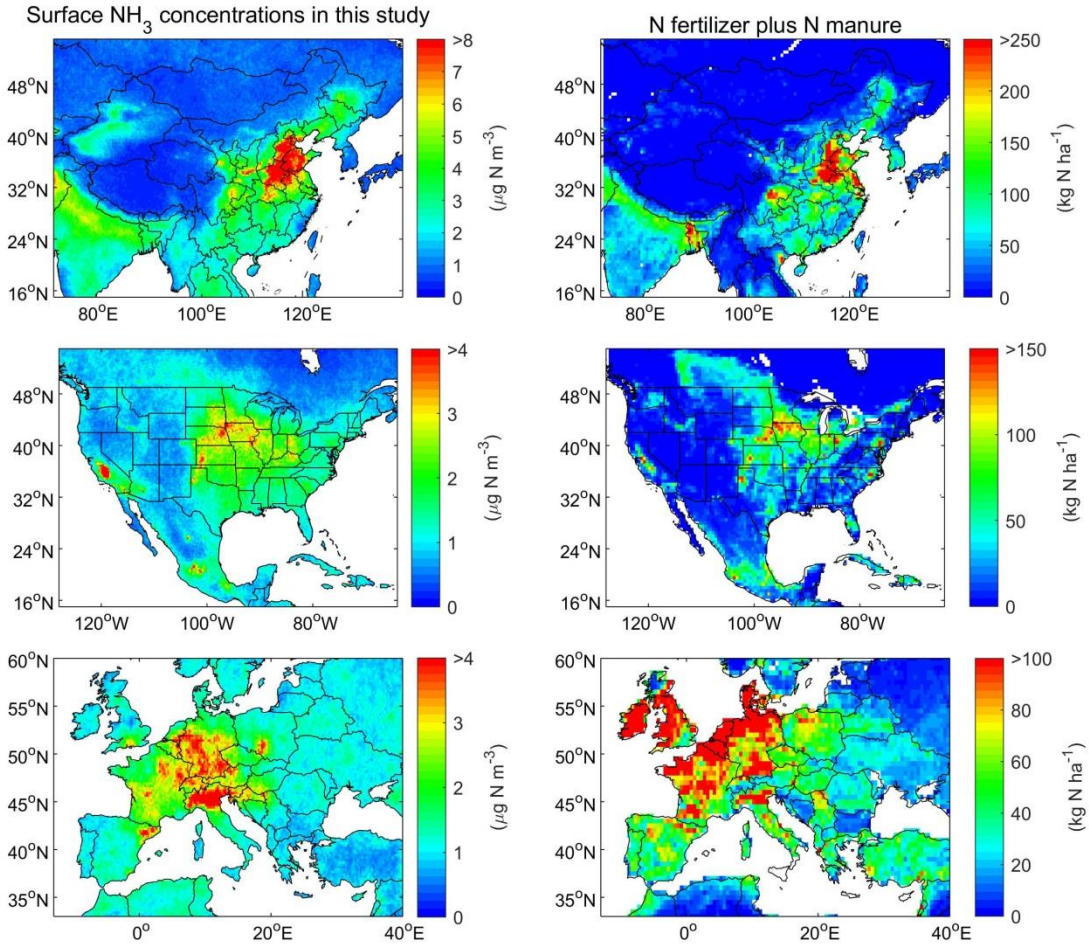

954

955 **Fig. 4** Spatial distribution of IASI-derived surface NH_3 concentrations, and N fertilizer plus N manure
956 (from N application) in China, Europe and US.

957

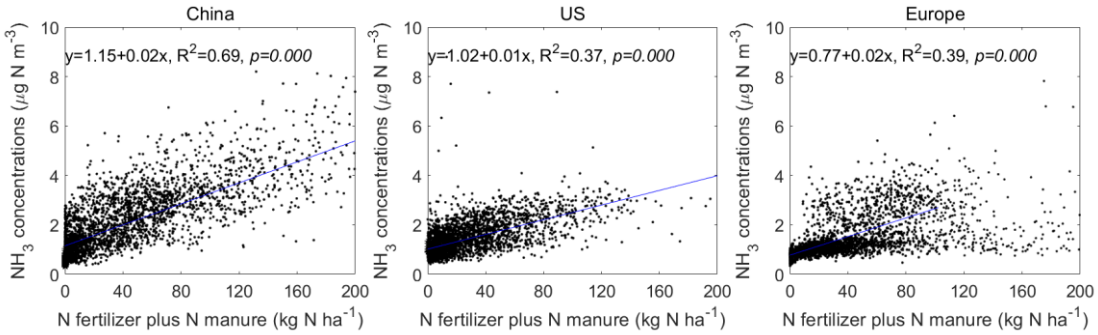

Fig. 5 Comparison of satellite-derived surface NH_3 concentrations and N fertilizer plus N manure (from N application) in China, US and Europe. The spatial resolution of satellite-derived surface NH_3 concentrations and N fertilizer plus N manure is 0.25^o and 0.5^o, respectively. We firstly resampled the satellite-derived surface NH_3 concentrations to 0.5^o grids, and then compared it with N fertilizer plus N manure by each grid cell. We obtained the N fertilizer and N manure data produced from McGill University (Potter et al., 2010).

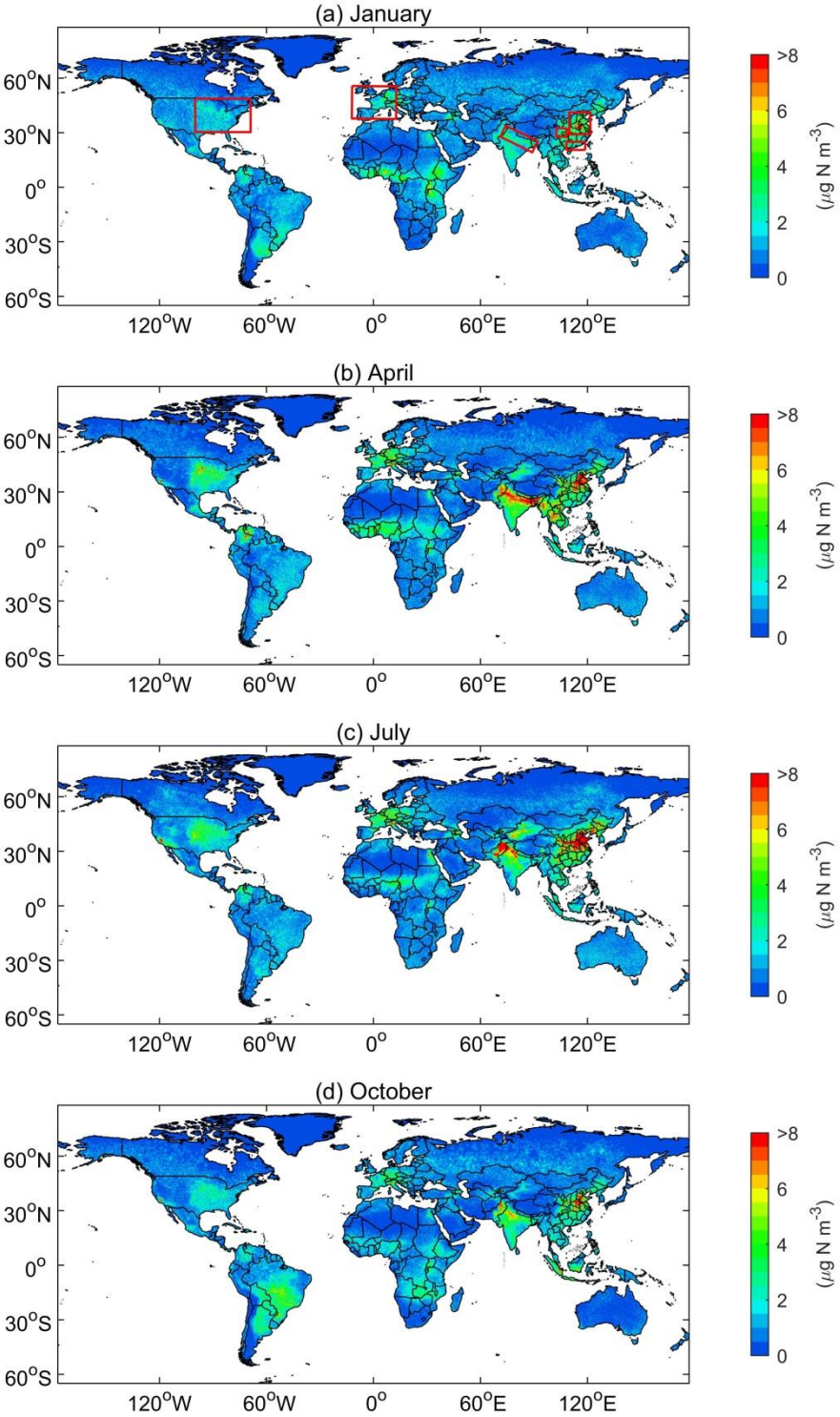

Fig. 6 Global surface NH_3 concentrations in January, April, July and October in 2014. The red rectangular regions include East China (ECH), Sichuan and Chongqing (SCH), Guangdong (GD), Northeast India (NEI), East US (EUS) and West Europe (WEU).

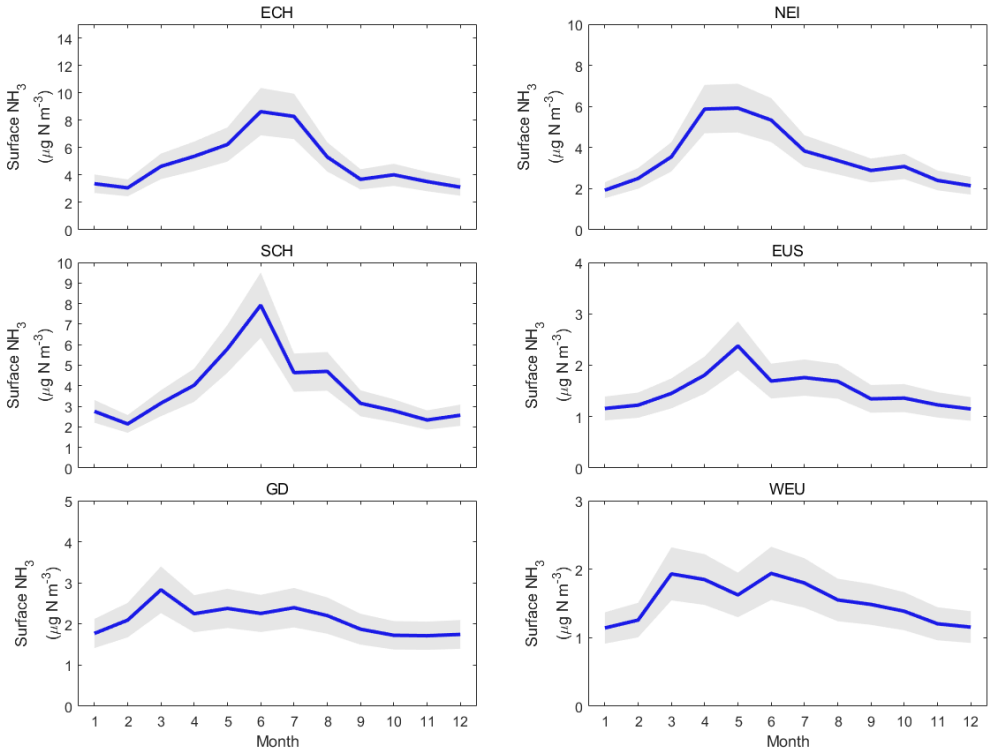

Fig. 7 Monthly variations of surface NH_3 concentrations in hotspot regions including East China (ECH), Sichuan and Chongqing (SCH), Guangdong (GD), Northeast India (NEI), East US (EUS) and West Europe (WEU).

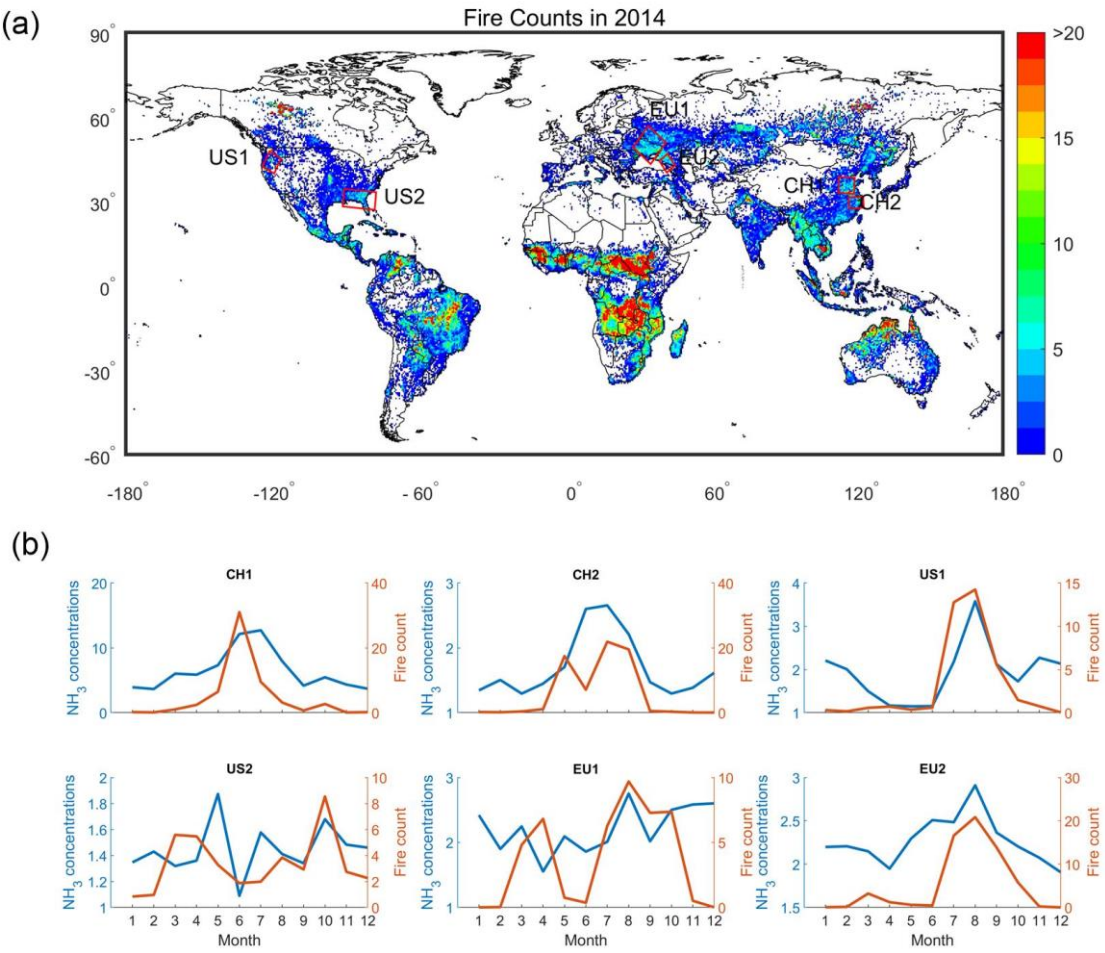

Fig. 8 MODIS fire counts in 2014. (a) Spatial distributions of MODIS fire counts. (b) Monthly variations of fire counts and surface NH_3 concentrations in biomass burning regions in China, the US and Europe.

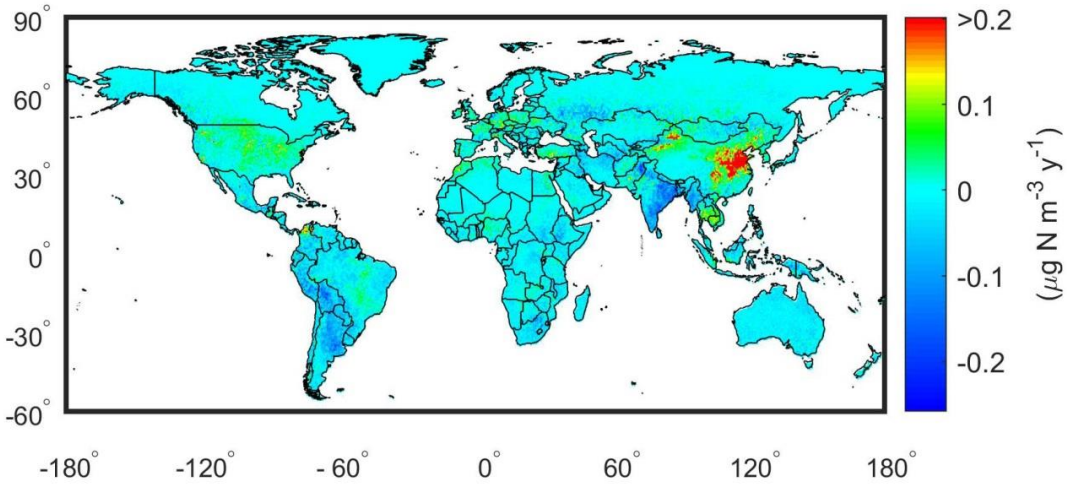

Fig. 9 Trends of IASI-derived surface NH_3 concentrations between 2008 and 2016. A linear regresion was perfomed to calculate the trends. The significance value (p) and R^2 for the trends can be found in **Fig. S10**.